The Effects of Packaged, but Misguided, Single-Stranded DNA Genomes Are Transmitted to the Outer Surface of the ϕX174 Capsid

Elizabeth T. Ogunbunmi,[a] Aaron P. Roznowski,[a] ⓘ Bentley A. Fane[a]

[a]The BIO5 Institute, University of Arizona, Tucson, Arizona, USA

ABSTRACT Most icosahedral viruses condense their genomes into volumetrically constrained capsids. However, concurrent genome biosynthesis and packaging are specific to single-stranded DNA (ssDNA) viruses. ssDNA genome packaging combines elements found in both double-stranded DNA (dsDNA) and ssRNA systems. Similar to dsDNA viruses, the genome is packaged into a preformed capsid. Like ssRNA viruses, there are numerous capsid-genome associations. In ssDNA microviruses, the DNA-binding protein J guides the genome between 60 icosahedrally ordered DNA binding pockets. It also partially neutralizes the DNA's negative phosphate backbone. ϕX174-related microviruses, such as G4 and α3, have J proteins that differ in length and charge organization. This suggests that interchanging J proteins could alter the path used to guide DNA in the capsid. Previously, a ϕXG4J chimera, in which the ϕX174 J gene was replaced with the G4 gene, was characterized. It displayed lethal packaging defects, which resulted in procapsids being removed from productive assembly. Here, we report the characterization of another inviable chimera, ϕXα3J. Unlike ϕXG4J, ϕXα3J efficiently packaged DNA but produced noninfectious particles. These particles displayed a reduced ability to attach to host cells, suggesting that internal DNA organization could distort the capsid's outer surface. Mutations that restored viability altered J-coat protein contact sites. These results provide evidence that the organization of ssDNA can affect both packaging and postpackaging phenomena.

IMPORTANCE ssDNA viruses utilize icosahedrally ordered protein-nucleic acids interactions to guide and organize their genomes into preformed shells. As previously demonstrated, chaotic genome-capsid associations can inhibit ϕX174 packaging by destabilizing packaging complexes. However, the consequences of poorly organized genomes may extend beyond the packaging reaction. As demonstrated herein, it can lead to uninfectious packaged particles. Thus, ssDNA genomes should be considered an integral and structural virion component, affecting the properties of the entire particle, which includes the capsid's outer surface.

KEYWORDS DNA packaging, bacteriophage, ϕX174, single-stranded DNA, virus assembly

As part of their life cycle, most icosahedral viruses must condense their genomes into volumetrically constrained capsids. Genome packaging and capsid assembly can occur sequentially or simultaneously. Single-stranded viral RNA (ssRNA) forms secondary structures that concurrently orchestrate packaging and assembly via protein-nucleic acid interactions (1, 2). In contrast, double-stranded DNA (dsDNA) genomes are packaged into preformed capsids. The packaged genome assumes the configuration of a cylindrical or spherical spool to accommodate the high nucleic acid density (3).

ssDNA viruses combine elements found in both the aforementioned systems. Similar to dsDNA viruses, the genome is packaged into a preformed capsid. However, ssDNA genome biosynthesis and packaging are simultaneous processes (4, 5). The parental strand is displaced

FIG 1 Characteristics of ϕX174 DNA packaging, DNA binding proteins, and their structural influences on packaged ssDNA. (A) ssDNA packaging. The parental strand, coated with J protein, is displaced into the capsid as the daughter strand is synthesized. (B) Ordered ssDNA (blue) and J proteins (purple and magenta) around a 5-fold axis of symmetry from ϕX174 filled with its own J protein (PDB 2BPA), α3 filled with its own J protein (PDB 1M06), and α3 filled with the ϕX174 J protein (PDB 1RB8). (C) ϕX174, G4, and α3 J proteins. The conserved C-terminal amino acids (blue) mediate coat-J protein interactions. The basic DNA-binding regions are depicted in magenta. The unique proline-rich region in ϕX174 is depicted in cyan.

into the procapsid as the daughter strand is synthesized (Fig. 1A). Reminiscent of the extensive capsid-nucleic acid associations seen in ssRNA viruses, packaged microvirus (ϕX174 et al.) genomes are partially ordered into 60 icosahedral DNA binding pockets (6–8). As seen in atomic structures (Fig. 1B), the DNA binding protein J appears to guide the genome between these pockets.

The ϕX174-like viruses are divided into three distinct clades, represented by the canonical species ϕX174, G4, and α3 (9–11). The amino acid sequences of their J proteins are depicted in Fig. 1C. The N termini are highly basic, whereas the C termini strongly interact with viral coat proteins (6–8). Although the basic amino acids neutralize DNA's negative charge, this may not be their primary role. The genome's negative charge far exceeds the positive charge of 60 J proteins. Thus, the ability to interact with the genome's phosphate backbone may be more critical in guiding the DNA into the capsid's icosahedral symmetry. Indeed, crystallographic observations made with ϕX174, α3, and α3 packaged with the ϕX174 J protein support protein J's influence on DNA organization (Fig. 1B). Altering the J protein alters the pattern of ordered DNA (6–8).

Although ϕX174 DNA replication and packaging have been extensively studied both *in vitro* and *in vivo* (4, 12–14), the function of the unessential A* protein remained poorly defined. Protein A* is a truncated version of the essential A protein, which mediates rolling circle replication. Similarly, A/A*-like arrangements are seen in some parvo- and circoviruses, encoding N-terminally truncated versions of their *Rep* proteins (15, 16). Recently, the ϕX174 A* protein was shown to play a quality control role during ssDNA packaging. Protein A*'s function was uncovered by characterizing packaging defects associated with a chimeric virus, ϕXG4J, in which the ϕX174 J gene was replaced with the G4 J gene. Presumably, protein A* slows DNA replication, ensuring that daughter strand synthesis does not outpace parental strand displacement (17). The larger ϕX174 J protein can complement G4 and α3 *null-J* mutants; however, the converse is not true (6, 17, 18). To determine whether a different chimeric virus would exhibit the same defects as ϕXG4J, ϕXα3J was generated and characterized. The results presented herein demonstrate that packaged particles with "misguided genomes" can display postpackaging defects.

RESULTS

The ϕXα3J chimera displays a complementation-dependent phenotype. ϕXα3J was constructed in a high-fidelity Q5 PCR. The α3 J sequence was divided between the

TABLE 1 Plating efficiency of ϕXα3J

Strain or genotype	Plating efficiency[a] with exogenous gene protein expression			
	None	ϕXJ	α3J	ϕXA*
Wild-type	1.2	1.0	1.0	1.0
ϕXα3J	6.8×10^{-5}	1.0	$<10^{-4}$	$<10^{-4}$
ϕX174 $am(J)$	$<10^{-4}$	1.0	$<10^{-4}$	ND
α3 $am(J)$	$<10^{-4}$	1.0^{-4}	1.0	ND
ϕXα3J $ins21^b$	$<10^{-4}$	1.0	ND	$<10^{-4}$

[a]Plating efficiency is defined as assay titer/titer with cloned ϕX174 J gene expression. ND, not determined.
[b]This strain contains a duplication of the protein A* target site, which rescues the lethal phenotype associated with the previously characterized ϕXG4J chimera.

5′ ends of two abutting primers, which do not anneal to the ϕX174 J gene in the ϕX174 template. However, the 3′ ends annealed to the upstream and downstream regions that surround the ϕX174 J gene. Thus, each end of the resulting linear PCR product contained one half of the α3 J gene. Circularization (see Materials and Methods) resulted in an intact α3 J gene situated where the ϕX174 gene once resided. The ribosome binding site for the J gene and the upstream promoters from which it is transcribed were not altered. Thus, gene expression presumably remained under wild-type ϕX174 control. Plaque formation required the exogenous expression of a cloned ϕX174 J gene (Table 1); thus, the chimera displayed a complementation-dependent phenotype. Rescue was species specific: only the cloned ϕX174 J gene supported ϕXα3J and ϕX174 $am(J)$ plaque formation. The plating efficiency of ϕXα3J and ϕX174 $am(J)$ on cells expressing the cloned α3 J gene was equal to the negative control, obtained by plating on cells with no plasmids. In contrast, exogenous α3 J gene expression rescued α3 $am(J)$, demonstrating that the cloned α3 J gene was functional. Therefore, the lethal phenotype was not an artifact of unforeseen reduced α3 J protein levels but a direct consequence of placing the α3 J protein into the ϕX174 system.

The ϕXα3J chimera formed uninfectious, packaged particles. To examine ϕXα3J infection products, lysis-resistant cells were infected at a multiplicity of infection (MOI) of 5.0 and incubated for 3 h at 37°C. Soluble extracts were prepared as described in Materials and Methods. Rate zonal sedimentation does not easily separate procapsids (108S) and virions (114S). To separate these two species, the external scaffolding protein was removed from procapsids by chloroform treatment. This results in unfilled degraded procapsids, which contain no DNA and sediment at 70S. After gradient fractionation, assembled particles were detected by UV spectroscopy.

As shown in Fig. 2A, the ϕXα3J 114S peak (pink) was not significantly reduced compared to the wild-type control (black). To determine specific infectivity (PFU/A_{260} unit), particles were titrated on cells expressing the cloned ϕX174 J gene: thus, any particle capable of infecting should have formed a plaque. The specific infectivity of ϕXα3J particles was reduced by more than 99% compared to wild-type virions: 3.5×10^9 PFU/A_{260} versus 7.9×10^{11} PFU/A_{260} unit, respectively (Table 2). The chimera's specific infectivity is likely much lower than 3.5×10^9 PFU/A_{260} unit. Specific infectivity was strictly defined as PFU/A_{260} unit regardless of the genotype of the PFU, which would include strains with second-site suppressors that had lost the complementation-dependent phenotype (see below).

The ssDNA genomes were extracted from purified wild-type and ϕXα3J particles and then examined by agarose gel electrophoresis (Fig. 2C). No significant differences in DNA migration or banding pattern were observed between the two samples. Although the G4 and α3 J proteins are similar in length (Fig. 1C), the two chimeras display very different defects. The previously characterized ϕXG4J chimera (17) exhibited severe stability defects during the packaging reaction, causing procapsids to dissociate or become insoluble. However, ϕXα3J particles appear to be genome filled but have lost the ability to interact with host cells (Fig. 2C and 3).

The ϕXα3J chimera exhibited defects early in the infection process. Errors in attachment or DNA penetration may explain why chimeric particles lacked infectivity. Typically, attachment studies rely on plaque assays, but ϕXα3J is not infectious. Thus, an attachment assay that relies on an SDS-PAGE analysis was developed. Equal
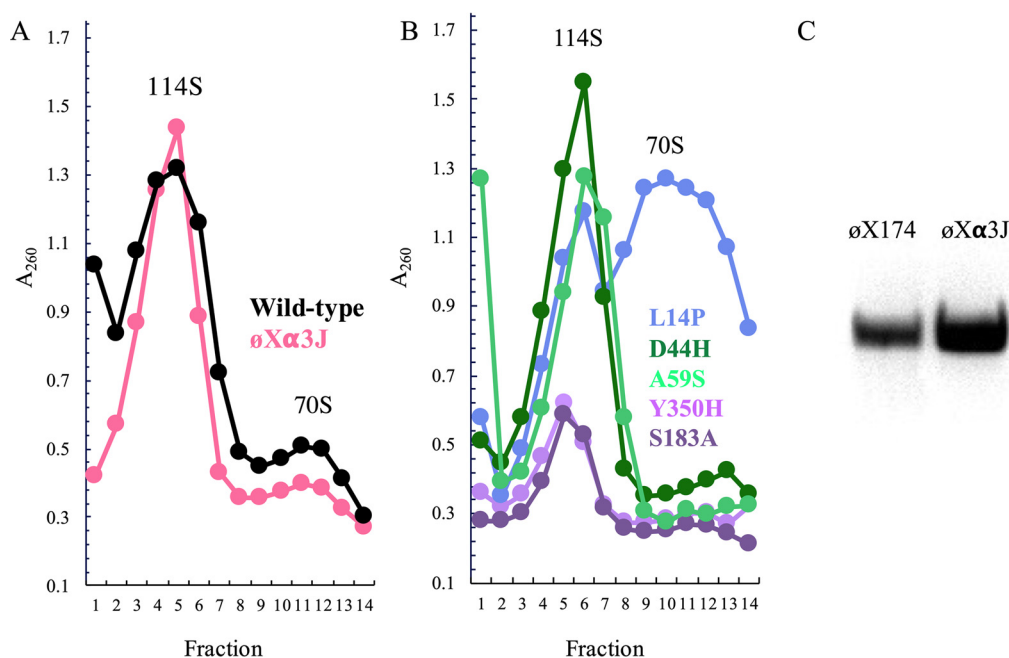
FIG 2 Biochemical characterization of $\phi X\alpha3J$ particles. (A) Sedimentation profiles of particles generated in wild-type- and $\phi X\alpha3J$-infected cells. Particles were detected by UV spectrophotometry of gradient fractions. The position of virions (114S) and degraded procapsids (70S) are indicated. (B) Sedimentation profiles of particles generated in su(J)/ $\phi X\alpha3J$-infected cells. The double mutant used in each experiment is given. All the infections for panels A and B were conducted on the same day. Thus, the wild-type and $\phi X\alpha3J$ samples depicted in panel A serve as the controls to which the curves in panel B can be directly compared. (C) Purified DNA extracted from wild-type and $\phi X\alpha3J$ 114S peaks from panel A.

amounts of wild-type and chimeric particles, based on A_{260} readings of purified samples, were incubated with host cells for 10 min. Afterwards samples were separated into supernatant and pellet fractions by centrifugation. The volume of the resuspended pellet and supernatant fractions were kept constant and analyzed side by side on an SDS-PAGE gel. Successful attachment should result in coat protein predominantly in the pellet with host cells. Attachment efficiency can be approximated by the ratio of coat protein within the pellet and supernatant fractions. The $\phi X\alpha3J$ supernatant samples displayed more coat protein than the pellet fraction compared to the wild-type control (Fig. 3A). The experiment was conducted twice with independently prepared input particles.

***E. coli* fails to efflux K$^+$ during $\phi X\alpha3J$ infection, indicating no penetration.** Although the above results suggest that $\phi X\alpha3J$ particles did not attach efficiently to host cells, attachment was not entirely inhibited. Moreover, the gel-based assay cannot

TABLE 2 Specific infectivity of suppressed $\phi X\alpha3J$ strains

Phage[a]	Specific infectivity (PFU/A_{260} unit)[b]	Infectivity normalized to wild type[c]
Wild type	7.9 ($\pm$ 2.7) $\times 10^{11}$	1.0 $\pm$ 0.3
$\phi X\alpha3J$	3.4 ($\pm$ 2.1) $\times 10^9$	<0.0043 $\pm$ 0.003
su(J)-F D44H/$\alpha3J$	1.4 ($\pm$ 0.1) $\times 10^{11}$	0.20 $\pm$ 0.01
su(J)-F A59S/$\alpha3J$	1.7 ($\pm$ 0.1) $\times 10^{11}$	0.20 $\pm$ 0.06
su(J)-F Y350H/$\alpha3J$	1.5 ($\pm$ 0.4) $\times 10^{11}$	0.20 $\pm$ 0.05
su(J)-H S183A/$\alpha3J$	1.4 ($\pm$ 0.6) $\times 10^{11}$	0.20 $\pm$ 0.07
su(J)-F L14P/$\alpha3J$	7.6 ($\pm$ 1.3) $\times 10^{10}$	0.10 $\pm$ 0.02

[a]Suppressing mutations are named with the gene in which the nucleotide substitution was found and the resulting amino acid change. Thus, su(J)-F D44H indicates a suppressor of J protein function [su(J)] in gene F (coat protein), conferring a D-to-H substitution at amino acid 44.
[b]The titers were determined on cells expressing a cloned wild-type $\phi X174$ J gene. Experiments were performed in triplicate. Standard deviations are given.
[c]Mutant specific infectivity/wild type specific infectivity.
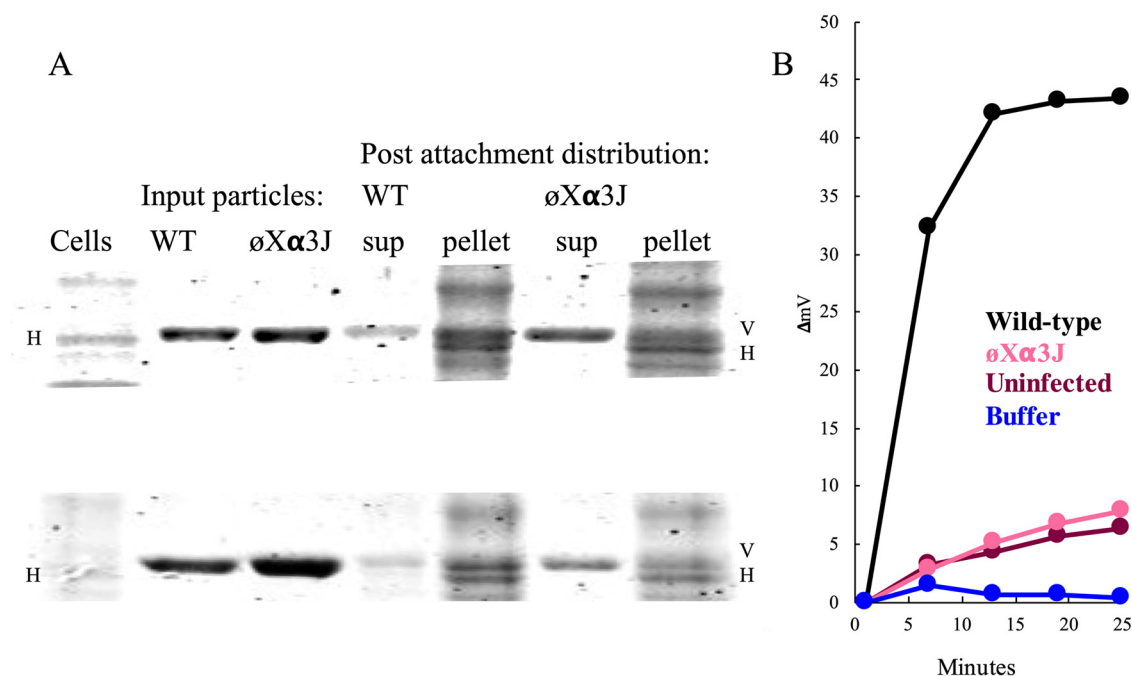
FIG 3 Characterization of virus-host interactions. (A) Distribution of the major coat protein in supernatant (sup) and pellet fractions after incubation with host cells. The coat protein was visualized by SDS-PAGE. Input particles reflect the total amount of particles before the addition of cells and separation into pellet and supernatant fractions. The two gels represent independent experiments conducted with independently generated and purified particles. The major coat migrates slightly more slowly than a host cell protein in the pellet fractions. V and H, coat and host protein, respectively. (B) Measurement of the K^+ efflux from host cells incubated with $\phi X174$ and $\phi X\alpha 3J$.

distinguish between specific and nonspecific attachment events. Therefore, the second stage of the viral life cycle, penetration, was also examined. Upon infection, phages form channels into cells for genome transport, which concurrently causes K^+ ions to efflux. Thus, penetration can be measured by changes in the extracellular K^+ ion concentration (19–22). As seen in Fig. 3B, K^+ efflux was readily apparent in the wild-type infection. In contrast, the K^+ efflux observed for the chimera infection did not significantly differ from that obtained from uninfected cells. These results indicate that $\phi X\alpha 3J$'s decreased infectivity is primarily due to defects in early viral-host interactions.

Second-site suppressors produce more infectious particles than the parental mutant. The results of second-site suppressor analyses can elucidate mechanistic details that may not be apparent from biochemical results alone. Thus, viable, complementation-independent $\phi X\alpha 3J$ variants were selected on cells without cloned $\phi X174$ gene J expression. Seven isolated suppressors contained missense substitutions in gene F, which encodes the viral coat protein, and one suppressor mutation resided in gene H. Protein H forms the tube for genome translocation. Table 3 summarizes these mutations, several of which were independently isolated multiple times. The variants were plated with and without exogenous J gene expression to calculate a plating efficiency, which was defined as the titer without exogenous J gene expression divided by the titer with exogenous J gene expression. Values ranged from 0.03 to 1.2 (Table 3), compared to 6.8×10^{-5} for the parental mutant.

To further characterize the suppressor strains, their infection products were analyzed by rate-zonal sedimentation. Three classes of mutants were defined by the sedimentation profiles. The first class includes the suppressors *su(J)-F D44H* and *su(J)-F A59S*, which have sedimentation profiles that resemble that of the wild type (Fig. 2B). These mutants displayed specific infectivities 2 orders of magnitude above that of the parental mutant but never reached wild-type levels (Table 2). This indicates that the suppressors elevate specific infectivity with no apparent negative effect on particle assembly or stability. In contrast, the second class of suppressors, *su(J)-F Y350H* and *su(J)-H S183A*, exhibited increased infectivity but severely reduced particle yields, suggesting that the suppressing mutations may have a

TABLE 3 Plating efficiency of suppressed ϕXα3J strains

Strain[a]	No. of independent isolates[b]	Plating efficiency with exogenous J protein expression[c]:	
		None	ϕXJ
Wild type	NA	1.2	1.0
ϕXα3J	NA	6.8×10^{-5}	1.0
su(J)-F L14P/α3J	1	0.50	1.0
su(J)-F G18V/α3J	3	1.1	1.0
su(J)-F L20F/α3J	3	0.50	1.0
su(J)-F D44H/α3J	3	0.60	1.0
su(J)-F A59S/α3J	1	1.2	1.0
su(J)-F T63A/α3J	3	0.03	1.0
su(J)-F Y350H/α3J	2	0.60	1.0
su(J)-H S183A/α3J	1	0.50	1.0

[a]Suppressing mutations are named with the gene in which the nucleotide substitution was found and the resulting amino acid change. Thus, su(J)-F D44H indicates a suppressor of J protein function [su(J)] in gene F (coat protein), conferring a D-to-H substitution at amino acid 44.
[b]The number of times the mutation was isolated from independently grown sources of ϕXα3J.
[c]Plating efficiency is defined as assay titer/titer with cloned ϕX174 J gene expression. NA, not applicable.

secondary defect affecting particle assembly. Lastly, su(J)-F L14P/ϕXα3J produced equal amounts of 114S and 70S particles. Accumulation of unfilled 70S particles occurs when capsids assemble but packaging does not commence (23, 24). The su(J)-F L14P mutation resides near the 3-fold axes of symmetry. In the procapsid, the 3-fold axes contain pores through which the DNA is packaged, after which the pores close. As seen with other mutations in this region of gene F, the introduction of a proline may lead to premature pore closure (23, 24).

The primary defect exhibited by ϕXα3J appeared to be different from that associated with ϕXG4J, i.e., instability of the packaging complex. Accordingly, the genetic mechanisms which suppress ϕXG4J's lethal phenotype failed to rescue ϕXα3J (17). ϕXG4J is rescued by overexpressing a cloned A* gene or by duplicating the protein's target site. The overexpression of the cloned A* gene had no effect on ϕXα3J plating efficiency (Table 1). In addition, the protein A* major target site was duplicated directly within the ϕXα3J genome (ϕXα3J ins21). Again, no rescue was observed (Table 1).

DISCUSSION

As described in the introduction, most icosahedral viruses must condense their genomes into volumetrically constrained capsids. In ϕX174, this process is mediated by genome interactions between J proteins and DNA binding pockets inside the capsid. The data presented herein and in a previous study (17) were generated using chimeric viruses, in which the endogenous J gene was replaced with a foreign J gene from a related species. Although similar to classical mutational studies, there are some key differences. Mutations may or may not alter the way a protein operates within a system. However, homologous proteins are functional in their own system but may have detrimental effects in a related species.

Biochemical analyses indicate that the primary defects associated with the chimeric viruses ϕXG4J and ϕXα3J are fundamentally different. The previously studied ϕXG4J chimera contains the smaller, less charged G4 J protein in the ϕX174 system (17). The chimera is unable to organize DNA into an optimal conformation during packaging, which results in the disappearance of virions from the 114S peak. If the G4 J protein is unable to optimally order DNA during packaging, it could destabilize the genome packaging complexes or cause them to aggregate.

The ϕXα3J chimera displayed a different defect. Particles were efficiently packaged, but infectivity was greatly reduced. In attachment assays, ϕXα3J associated with cells less efficiently than the wild type. Those particles that did associate did not appear to penetrate. This may indicate that the cell-associated particles were making nonspecific interactions. Although the precise mechanistic details are unknown, the internal organization of the genome appears to be affecting the capsid's external surface, which has been previously observed in other genetic and biophysical studies (6, 25, 26).
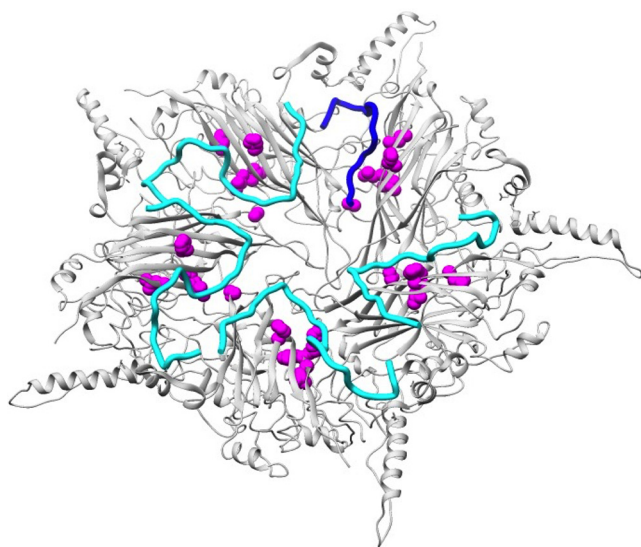
FIG 4 The coat protein suppressors of ϕXα3J. The coat protein is depicted in gray; the suppressors are in magenta. The ϕX174 J protein is depicted in cyan. In one asymmetric unit, the α3J protein (blue) was modeled into the ϕX174 structure.

Compensatory mutations reflect different primary biochemical defects. Second-site suppressor mutations can provide further mechanistic insights. The second-site suppressors of ϕXG4J duplicated the J-F intercistronic region, which contains protein A*'s primary target site. Accordingly, the chimera was rescued by elevating intracellular protein A* concentrations (17). The A* protein is a truncated version of the A protein. Unlike protein A, protein A* inhibits DNA synthesis by preventing the unwinding of the two parental strands (27). Restoration of viability may be due to the stabilizing effects of coordinating genome synthesis and packaging. In contrast, excess A* protein did not rescue ϕXα3J, nor did the duplication of its target site. Instead, the second-site suppressors of ϕXα3J conferred changes in the viral coat and DNA pilot proteins. All second-site suppressors elevated specific infectivity to values approaching, but not quite reaching, wild-type levels. Some suppressors conferred secondary assembly defects.

As shown in Fig. 4, most second-site suppressor mutations alter amino acid residues on the inner surface of the coat protein. Moreover, they line the path taken by protein J in the virion. Three of the residues—L14, A59, and D44H—are known to make direct contact with the J protein. The other residues are directly adjacent to J protein contact sites. This suggests that these suppressors may modify packaged genome organization, via coat-J protein interactions, to produce more infectious particles. Despite using several independently produced parental populations in both studies, no suppressing mutations were found in gene J. This suggests that the foreign J proteins have diverged too much from the ϕX174 protein to adapt to the ϕX174 system via single intragenic mutations. In contrast, the coat proteins exhibit much more amino acid homology and highly superimposable 3D structures (8, 28, 29).

The mechanism by which the second-site suppressor in protein H restores infectivity is more obscure. Protein H first assumes a monomeric conformation for incorporation during procapsid assembly, an event that occurs before packaging (30). After attachment, 10 monomers form a DNA translocating tube that emerges from a 5-fold axis of symmetry (31, 32). At least two major conformational changes must occur. (i) The H proteins must oligomerize, and (ii) the coat proteins must rearrange to form a pore through which the tube emerges. If ϕXα3J virions are more rigid or are kinetically trapped due to suboptimal genome organization, these conformational changes may be impeded. As seen in Fig. 2B, the *su(J)-H* mutation greatly reduces particle yields, which complicated further analyses. Thus, any interpretation is speculative.

Primary versus secondary φXG4J defects. The primary defects associated with φXG4J and φXα3J differ; however, the second-site suppressors of φXα3J may provide insights into a secondary φXG4J defect. Although most φXG4J packaging complexes dissociate, a small number of virions are produced. These particles, like φXα3J, exhibit a reduced specific infectivity (17). The strong suppressors of φXG4J duplicate the A* protein's target site, which affects the packaging reaction: however, a class of very weak suppressors were also identified in the viral coat protein (17). Like the suppressors of φXα3J, these were at J-coat protein contact sites. Two of them contained identical amino acid substitutions at L14 and D44.

Function of the J protein's positively charged residues. Traditionally, the function of the J protein basic residues was considered DNA charge neutralization (33, 34). While neutralization is likely one role, J protein's positively charged residues may be more critical in guiding the DNA to ensure orderly packaging and genome organization. Several observations support this hypothesis. φX174 has the smallest genome of the φX174-like viruses but contains the most basic J protein (+12). In addition, chimeras with second-site suppressors can produce infectious particles filled with G4 (+6) and α3 (+7) J proteins. Several G4 and α3 codons could mutate, via one nucleotide change, to encode a basic amino acid. Theoretically, this would enhance the charge-neutralization function. However, such suppressors were never isolated. Moreover, many of the φXα3J suppressing substitutions (Table 3) would have little to no effect on the electrostatic potential of the capsid's inner surface. Thus, the larger φX174 J protein may be required to guide DNA over a negatively charged patch in the coat protein that is not found in either G4 and α3 (6). In conclusion, the nature of the suppressing mutations in both chimeras may be more indicative of J protein's guiding function.

MATERIALS AND METHODS

Phage plating, media, buffers, stock preparation, and bacterial strains. The plating protocol, media, buffers, stock preparation, and the wild-type *Escherichia coli* C strain C122 have been previously described (35).The RY7211 cell line contains a mutation in the *mraY* gene, conferring resistance to viral E protein-mediated lysis (36).

Cloned genes used in these studies. Like the previously described cloned φX174 J and G4 J genes (17), the α3 J gene was PCR amplified using primers that introduced upstream NcoI and downstream HindIII sites. The resulting fragments were digested with NcoI and HindIII and ligated into pSE420 (Invitrogen) treated with the same enzymes. Gene expression was induced by the addition of IPTG (isopropyl-β-D-thiogalactopyranoside) to a concentration of 0.1 mM. The cloning of the φX174 A* gene into pBAD33 (Thermo Fisher) has been previously described (17). Gene expression was induced by supplementing media with 0.2% arabinose and then repressed by supplementing media with 0.2% glucose.

ssDNA, RF dsDNA, assembled particle-associated DNA purification and extracts for sucrose gradient sedimentation. The ssDNA was generated and purified with the OLT (our little trick) protocol, which has been previously described in detail (37), as has the protocol used for replicative-form (RF) dsDNA purification (38). To isolate DNA associated with assembled particles, gradient fractions containing 90S to 150S particles were diluted 5-fold in 10 mM Tris-HCl (pH 7.5)–10 mM NaCl–1.0 mM EDTA. Sodium dodecyl sulfate (SDS), pronase, and additional EDTA were added to respective final concentrations of 0.5% (wt/vol), 0.5 mg/ml, and 10 mM. Samples were incubated at 37℃ for 2.5 h before being extracted as previously described (17). Sucrose gradient preparation, particle isolation, and infected cell extracts were described previously (24, 25). Briefly, 100 ml of lysis-resistant cells was infected at a multiplicity of infection (MOI) of 3.0 and incubated for 3 h at 37℃. Infected cells were concentrated and resuspended in 3.0 ml sucrose gradient buffer (SGB; 100 mM NaCl, 5.0 mM EDTA, 6.4 mM Na_2HPO_4, 3.3 mM KH_2PO_4 [pH 7.0]) and then lysed by an overnight incubation with lysozyme (2.0 mg/ml). After removing cellular debris, the supernatant was concentrated to 200 μl in a Corning Spin-X spin column (100-kDa cutoff) and loaded atop a 5.0-ml, 5-to-30% sucrose gradient (wt/vol). Gradients were spun at 192,000 × *g* for 1 h and then fractionated into 125-μl fractions. Assembled particles were detect by UV spectroscopy (A_{260} and A_{280}).

Construction of the φXα3J chimeric genome. φXα3J was constructed in a high-fidelity Q5 PCR (New England Biolabs). The reaction was designed to replace the φX174 J gene with that of α3. The α3 J sequence was divided between the 5′ ends of two abutting primers, which do not anneal to the φX174 J gene in the φX174 template. However, the 3′ ends annealed to the upstream and downstream regions that surround the φX174 J gene. Thus, each end of the resulting linear PCR product contained one half of the α3 J gene. After the product's 5′ hydroxyl termini were phosphorylated with T4 polynucleotide kinase, the molecule was circularized by ligating the ends. This results in an intact α3 J gene situated where the φX174 gene once resided. The mutant was recovered in cells expressing the φX174J gene. To generate φXα3J + 21, φX174 + 21 DNA served as the template in the Q5 polymerase reactions. The α3J gene was introduced and the φX174 J gene removed as described above.

K+ efflux assay. The protocol for the efflux assay was originally described for bacteriophage T5 (19) and was adapted to the $\phi X\alpha 3J$ and $\phi X174$ system as previously described (21, 22).

Attachment assay for noninfectious particles. A 1-ml aliquot of fresh C122 overnight cell culture was washed in 1 ml of the lab's standard dilution HFB buffer (0.06 M NH_4Cl–0.09 M NaCl–0.1 M KCl–0.1 M Tris-HCl [pH 7.4]–1.0 mM $MgSO_4$–l.0 mM $CaCl_2$), spun down, and resuspended in 1 ml of HFB further supplemented by 10 mM $MgCl_2$ and 5.0 mM $CaCl_2$. One hundred microliters of cells was infected with 60 μl of a phage preparation with an A_{260} value corresponding to $\sim$1.0 × 10^{12} PFU/ml for infectious particles. Samples were incubated at 37°C for 10 min. The cells and phage were centrifuged, and the supernatant was immediately removed and further concentrated to 50 μl in a Corning Spin-X spin column with a 30-kDa molecular weight cutoff. The pellet was resuspended in 50 μl H_2O before analysis by SDS-PAGE.

REFERENCES

1. Gopal A, Egecioglu DE, Yoffe AM, Ben-Shaul A, Rao AL, Knobler CM, Gelbart WM. 2014. Viral RNAs are unusually compact. PLoS One 9: e105875. https://doi.org/10.1371/journal.pone.0105875.

2. Speir JA, Johnson JE. 2012. Nucleic acid packaging in viruses. Curr Opin Struct Biol 22:65–71. https://doi.org/10.1016/j.sbi.2011.11.002.

3. Cerritelli ME, Studier FW. 1996. Assembly of T7 capsids from independently expressed and purified head protein and scaffolding protein. J Mol Biol 258:286–298. https://doi.org/10.1006/jmbi.1996.0250.

4. Aoyama A, Hamatake RK, Hayashi M. 1981. Morphogenesis of phi X174: in vitro synthesis of infectious phage from purified viral components. Proc Natl Acad Sci U S A 78:7285–7289. https://doi.org/10.1073/pnas.78.12.7285.

5. King JA, Dubielzig R, Grimm D, Kleinschmidt JA. 2001. DNA helicase-mediated packaging of adeno-associated virus type 2 genomes into preformed capsids. EMBO J 20:3282–3291. https://doi.org/10.1093/emboj/20.12.3282.

6. Bernal RA, Hafenstein S, Esmeralda R, Fane BA, Rossmann MG. 2004. The phiX174 protein J mediates DNA packaging and viral attachment to host cells. J Mol Biol 337:1109–1122. https://doi.org/10.1016/j.jmb.2004.02.033.

7. McKenna R, Ilag LL, Rossmann MG. 1994. Analysis of the single-stranded DNA bacteriophage phi X174, refined at a resolution of 3.0 A. J Mol Biol 237:517–543. https://doi.org/10.1006/jmbi.1994.1253.

8. McKenna R, Xia D, Willingmann P, Ilag LL, Krishnaswamy S, Rossmann MG, Olson NH, Baker TS, Incardona NL. 1992. Atomic structure of single-stranded DNA bacteriophage phi X174 and its functional implications. Nature 355:137–143. https://doi.org/10.1038/355137a0.

9. Godson GN, Barrell BG, Staden R, Fiddes JC. 1978. Nucleotide sequence of bacteriophage G4 DNA. Nature 276:236–247. https://doi.org/10.1038/276236a0.

10. Kodaira K, Nakano K, Okada S, Taketo A. 1992. Nucleotide sequence of the genome of the bacteriophage alpha 3: interrelationship of the genome structure and the gene products with those of the phages, phi X174, G4 and phi K. Biochim Biophys Acta 1130:277–288. https://doi.org/10.1016/0167-4781(92)90440-B.

11. Sanger F, Coulson AR, Friedmann T, Air GM, Barrell BG, Brown NL, Fiddes JC, Hutchison CA, III, Slocombe PM, Smith M. 1978. The nucleotide sequence of bacteriophage phiX174. J Mol Biol 125:225–246. https://doi.org/10.1016/0022-2836(78)90346-7.

12. Aoyama A, Hamatake RK, Hayashi M. 1983. In vitro synthesis of bacteriophage phi X174 by purified components. Proc Natl Acad Sci U S A 80:4195–4199. https://doi.org/10.1073/pnas.80.14.4195.

13. Kornberg A. 1980. DNA replication. Freeman, San Francisco, CA.

14. Kornberg A. 1982. Supplement to DNA replication. Freeman, San Francisco, CA.

15. Chejanovsky N, Carter BJ. 1989. Mutagenesis of an AUG codon in the adeno-associated virus rep gene: effects on viral DNA replication. Virology 173:120–128. https://doi.org/10.1016/0042-6822(89)90227-4.

16. Mankertz A, Hillenbrand B. 2001. Replication of porcine circovirus type 1 requires two proteins encoded by the viral rep gene. Virology 279:429–438. https://doi.org/10.1006/viro.2000.0730.

17. Roznowski AP, Doore SM, Kemp SZ, Fane BA. 2020. Finally, a role befitting Astar: the strongly conserved, unessential microvirus A* proteins ensure the product fidelity of packaging reactions. J Virol 94:e01593-19. https://doi.org/10.1128/JVI.01593-19.

18. Fane BA, Head S, Hayashi M. 1992. Functional relationship between the J proteins of bacteriophages phi X174 and G4 during phage morphogenesis. J Bacteriol 174:2717–2719. https://doi.org/10.1128/jb.174.8.2717-2719.1992.

19. Boulanger P, Letellier L. 1992. Ion channels are likely to be involved in the two steps of phage T5 DNA penetration into Escherichia coli cells. J Biol Chem 267:3168–3172. https://doi.org/10.1016/S0021-9258(19)50710-4.

20. Cumby N, Reimer K, Mengin-Lecreulx D, Davidson AR, Maxwell KL. 2015. The phage tail tape measure protein, an inner membrane protein and a periplasmic chaperone play connected roles in the genome injection process of E. coli phage HK97. Mol Microbiol 96:437–447. https://doi.org/10.1111/mmi.12918.

21. Roznowski AP, Fisher JM, Fane BA. 2020. Mutagenic analysis of a DNA translocating tube's interior surface. Viruses 12:670. https://doi.org/10.3390/v12060670.

22. Roznowski AP, Young RJ, Love SD, Andromita AA, Guzman VA, Wilch MH, Block A, McGill A, Lavelle M, Romanova A, Sekiguchi A, Wang M, Burch AD, Fane BA. 2019. Recessive host range mutants and unsusceptible cells that inactivate virions without genome penetration: ecological and technical implications. J Virol 93:e01767-18. https://doi.org/10.1128/JVI.01767-18.

23. Uchiyama A, Chen M, Fane BA. 2007. Characterization and function of putative substrate specificity domain in microvirus external scaffolding proteins. J Virol 81:8587–8592. https://doi.org/10.1128/JVI.00301-07.

24. Uchiyama A, Fane BA. 2005. Identification of an interacting coat-external scaffolding protein domain required for both the initiation of phiX174 procapsid morphogenesis and the completion of DNA packaging. J Virol 79:6751–6756. https://doi.org/10.1128/JVI.79.11.6751-6756.2005.

25. Hafenstein S, Fane BA. 2002. phi X174 genome-capsid interactions influence the biophysical properties of the virion: evidence for a scaffolding-like function for the genome during the final stages of morphogenesis. J Virol 76:5350–5356. https://doi.org/10.1128/jvi.76.11.5350-5356.2002.

26. Hafenstein SL, Chen M, Fane BA. 2004. Genetic and functional analyses of the oX174 DNA binding protein: the effects of substitutions for amino acid residues that spatially organize the two DNA binding domains. Virology 318:204–213. https://doi.org/10.1016/j.virol.2003.09.018.

27. Eisenberg S, Ascarelli R. 1981. The A* protein of phi X174 is an inhibitor of DNA replication. Nucleic Acids Res 9:1991–2002. https://doi.org/10.1093/nar/9.8.1991.

28. Bernal RA, Hafenstein S, Olson NH, Bowman VD, Chipman PR, Baker TS, Fane BA, Rossmann MG. 2003. Structural studies of bacteriophage alpha3 assembly. J Mol Biol 325:11–24. https://doi.org/10.1016/s0022-2836(02)01201-9.

29. McKenna R, Bowman BR, Ilag LL, Rossmann MG, Fane BA. 1996. Atomic structure of the degraded procapsid particle of the bacteriophage G4: induced structural changes in the presence of calcium ions and functional implications. J Mol Biol 256:736–750. https://doi.org/10.1006/jmbi.1996.0121.

30. Cherwa JE, Jr, Organtini LJ, Ashley RE, Hafenstein SL, Fane BA. 2011. In vitro assembly of the oX174 procapsid from external scaffolding protein oligomers and early pentameric assembly intermediates. J Mol Biol 412:387–396. https://doi.org/10.1016/j.jmb.2011.07.070.

31. Sun L, Young LN, Zhang X, Boudko SP, Fokine A, Zbornik E, Roznowski AP, Molineux IJ, Rossmann MG, Fane BA. 2014. Icosahedral bacteriophage PhiX174 forms a tail for DNA transport during infection. Nature 505:432–435. https://doi.org/10.1038/nature12816.

32. Sun Y, Roznowski AP, Tokuda JM, Klose T, Mauney A, Pollack L, Fane BA, Rossmann MG. 2017. Structural changes of tailless bacteriophage PhiX174

during penetration of bacterial cell walls. Proc Natl Acad Sci U S A 114:13708–13713. https://doi.org/10.1073/pnas.1716614114.

33. Hamatake RK, Aoyama A, Hayashi M. 1985. The J gene of bacteriophage phi X174: in vitro analysis of J protein function. J Virol 54:345–350. https://doi.org/10.1128/JVI.54.2.345-350.1985.

34. Jennings B, Fane BA. 1997. Genetic analysis of the phi X174 DNA binding protein. Virology 227:370–377. https://doi.org/10.1006/viro.1996.8351.

35. Fane BA, Hayashi M. 1991. Second-site suppressors of a cold-sensitive prohead accessory protein of bacteriophage phi X174. Genetics 128:663–671. https://doi.org/10.1093/genetics/128.4.663.

36. Bernhardt TG, Struck DK, Young R. 2001. The lysis protein E of phi X174 is a specific inhibitor of the MraY-catalyzed step in peptidoglycan synthesis. J Biol Chem 276:6093–6097. https://doi.org/10.1074/jbc.M007638200.

37. Blackburn BJ, Li S, Roznowski AP, Perez AR, Villarreal RH, Johnson CJ, Hardy M, Tuckerman EC, Burch AD, Fane BA. 2017. Coat protein mutations that alter the flux of morphogenetic intermediates through the phiX174 early assembly pathway. J Virol 91:e01384-17. https://doi.org/10.1128/JVI.01384-17.

38. Burch AD, Ta J, Fane BA. 1999. Cross-functional analysis of the Microviridae internal scaffolding protein. J Mol Biol 286:95–104. https://doi.org/10.1006/jmbi.1998.2450.